ADDING SURVEILLANCE CAPABILITIES TO A LEO TRACKER USING A LOW-COST WIDE FIELD OF VIEW DETECTION SYSTEM

Radu Danescu[(1)], Razvan Itu[(1)], Vlad Turcu[(2)], Dan Moldovan[(2)]

[(1)] Technical University of Cluj-Napoca, Str. Memorandumului 28, Cluj-Napoca, Romania, Email: {radu.danescu, razvan.itu}@cs.utcluj.ro
[(2)] Romanian Academy Cluj-Napoca Branch, Astronomical Observatory Cluj-Napoca, Str. Ciresilor 19, Cluj-Napoca, Romania, Email: {vladturcu, dan.moldovan}@academia-cj.ro

ABSTRACT

The Astronomical Observatory of Cluj-Napoca is involved in the European SST effort, using its telescopes to track satellites of various orbits. The narrow field of view of the observation system limits the system to tracking operations. We aim to add surveillance capabilities to the observation system, using the idle time between tracking exposures. We have designed and implemented a low-cost wide field of view observation system that operates in staring mode. The software is able to control the acquisition process, detect the satellite streaks, build tracklets, and perform astrometric reduction. For each tracklet, predictions in RA/DEC coordinates are generated one minute ahead by extrapolating the detected trajectories. One prediction is sent via a radio interface to the computer controlling the telescope system. The end result is a system of increased throughput while maintaining the measurement accuracy of the telescope.

1 INTRODUCTION

The Low Earth Orbit contains thousands of objects, their number increasing day by day. Many of these objects are useful, but many are inactive satellites, leftovers from old launches, or fragments of destroyed satellites. The resident objects that have no active purpose are called space debris, and their continuous observation and cataloguing is extremely useful [1], [2].

The sensor of choice for keeping an eye on the low Earth orbit is the RADAR. Large antenna arrays such as Space Fence System [3] update daily the orbital data for thousands of objects. However, the radar solution is costly, requiring vast amounts of hardware and power, therefore being the privilege of powerful nations and military establishments.

Optical systems, on the other hand, are passive receptors of light, and use optical instruments cameras and image processing algorithms to detect passing targets. While they are not able to directly infer the distance, they can produce accurate angular coordinates.

There are two main methods to observe orbiting objects using optical sensors, covered by the generic term Space Surveillance and Tracking (SST). The tracking method uses the known orbital elements to predict the trajectories, and a narrow field of view (FOV), accurate instrument is pointed towards the predicted region of the sky, the observations are made, and the orbit is updated based on the observations. This approach works with known objects with stable orbits. Even more, some tracking approaches use the orbital elements to lock the telescope on the orbiting object, making it appear as a bright point against a moving starry background. For this approach the orbital elements of the tracked target must be up to date. The results of tracking methods are usually very precise, but the main disadvantage is the dependence on known orbital parameters.

The other observation strategy is surveillance. This approach is able to detect and track targets with known and also with unknown orbital parameters, by observing the sky with a large FOV instrument or an array of instruments that together form a larger FOV [4], [5]. The surveillance approaches are able to detect many more targets, but they either require a lot more processing power and hardware, to get accurate angular measurements (by processing either multiple images, or images of very high resolution), or they produce less accurate results due to the larger angular pixel size of the acquired image [6].

A method that combines the advantages of surveillance and tracking is “Stare and Chase”, where the target is first acquired by a larger FOV instrument, and then it is passed to a narrower instrument for tracking [7]. While some systems are specifically designed for this mode of operation, the work that we’ll present in this paper aims to add stare and chase functionality to an existing system, with minimum intervention upon the system’s hardware setup and without interfering with the system’s existing capabilities.

2 SUMMARY OF THE WORK

The Astronomical Observatory of Cluj-Napoca, using the Feleacu observation site (latitude 46.71040333 N, longitude 23.593594666 E, altitude 787.560 m), is involved in the European SST effort, using its telescopes

Proc. 2nd NEO and Debris Detection Conference, Darmstadt, Germany, 24-26 January 2023, published by the ESA Space Safety Programme Office
Ed. T. Flohrer, R. Moissl, F. Schmitz (http://conference.sdo.esoc.esa.int, February 2023)

to track satellites of various orbits. For the Low Earth Orbit (LEO) satellites, the Observatory's team uses the Orion ShortTube 80 refractor telescope, mounted on the fast-moving PlaneWave L600 equatorial mount system, and the images are captured using the SBIG STT 1603ME CCD camera in binning mode, allowing a frame capture rate of 30 frames a minute, and an angular measurement error of less than 10 arcseconds.

The narrow FOV of the system, 1.98x1.32 degrees, limits the system to tracking operations. The objective of the work presented in this paper is to add surveillance capabilities to the observation system, using the idle time between tracking exposures to capture other passing satellites. For this purpose, we have designed and implemented a low-cost wide FOV observation system, based on off the shelf components: one 13-inch 2020 MacBook Pro laptop, one Canon EOS 800D DSLR camera, configured to provide 2400x1600 pixel images and working in external triggering, pulse width exposure control mode ("Bulb" mode), and a synchronization device based on a GPS receiver and an Arduino microcontroller, for precise timestamping of the acquired images. The low-cost wide FOV system has a 60x40 degrees FOV, and can be set up anywhere in less than 10 minutes. The system operates in staring mode; therefore, no specific mount is needed, only a small, basic tripod for the camera.

The software running on the laptop is able to control the acquisition process, detect the satellite streaks, build tracklets and perform astrometric reduction with a frame rate of 10 frames a minute. For each tracklet, predictions are generated one minute ahead by extrapolating the detected trajectories. From all predictions generated at one time, the one resulting from the oldest track is selected to be sent to the main observation system to position the telescope.

The wide FOV system sends one set of coordinates, comprised of Right Ascension and Declination, to the telescope-based system, using a serial-over-radio interface (HC-12, 433 MHz). The interface works reliably at hundreds of meters, allowing flexibility in the placing of the wide FOV system. The angular errors of the wide FOV predictions are between 90 and 200 arcseconds, a large error for a surveillance/tracking system, but which guarantees that the telescope will be oriented well enough that the target will enter its field of view, as the FOV of the telescope is much wider than the prediction error.

The prediction for surveillance mechanism does not interfere with the tracking process. When tracking, the telescope controlling software will ignore the radio messages from the wide FOV system, but otherwise it will make use of the available time to observe targets acquired in the large FOV.

3 SYSTEM DESCRIPTION

The whole tracking and surveillance system is based on two main sub-systems: the wide FOV system operating in staring mode, and the narrow FOV system operating in sidereal tracking mode.

The wide FOV system is set up outside of the main dome of the Observatory, on a simple, rigid surface. There are no other requirements, no specialized mount, no power source and no cable connection to the main dome is necessary. The narrow FOV system is placed in the main dome of the Observatory. The placement of the two subsystems, overlayed on a Google Maps satellite view, is shown in Figure 1.

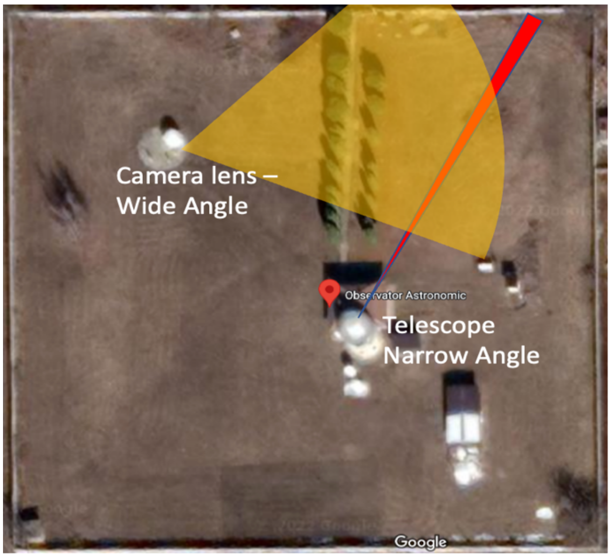

Figure 1. Placement of the two observation systems.

The wide FOV system has the following hardware components:

Camera: Canon EOS 800 D, using external trigger signal with pulse width exposure time control. The image size is 2400x1600 pixels.

Lens: Sigma EXDG 20 mm F/1.8. With the camera above, the effective FOV is 60x40 degrees, and the angular resolution is 90 arcseconds/pixel.

Portable computer: 13-inch MacBook Pro 2020, equipped with Apple Silicon M1 processor. The computer controls the acquisition and processes the images in real time, and provides power for all other components with the exception of the camera, which has its own accumulator.

GPS-based synchronization device: a microcontroller based device connected to the computer via the USB bus, receives the trigger command and the exposure duration, and synchronizes it with the global time read using the UART and the 1PPS interface of the GPS receiver.

Radio communication interface: a HC-12 radio transceiver using the 433 MHz frequency, has a UART interface operating at 9600 bps. The UART interface is interfaced with the computer using a FT232 USB to UART adapter.

The narrow FOV system has the following hardware components:

Telescope: Orion ShortTube 80 refractor telescope.

Camera: SBIG STT 1603ME CCD camera, working in binning mode, producing 16-bit FITS images of 768x512 pixels every 2 seconds, one second being for exposure and the other second for data transfer.

Telescope mount: PlaneWave L600, a fast-moving accurate equatorial mount, with ASCOM compatible software interface which allows real time positioning based on received predicted coordinates.

Timestamping device: Synoptes [8] precise timestamping device, based on GPS, able to assign microsecond-accurate timestamps to the acquired images.

Radio receiver unit: a microcontroller-based device for receiving the predicted coordinates. It contains a HC-12 radio transceiver. This unit has also an additional function of interfacing the narrow FOV system's compute with the dome control unit.

Dome control unit: a microcontroller and relay-based device for controlling the driving motors of the Observatory's dome. The dome's 15 degrees opening is not enough for allowing unimpeded observations for all the areas the telescope is commanded to cover, and therefore the dome must be also automatically rotated. The dome itself is built in the 1970s, and does not have intrinsic automation capabilities.

Computer: generic PC equipped with software for image acquisition and timestamping, and with custom software for receiving the prediction signals, and for commanding the telescope and the dome.

The architecture of the two systems is shown in Figure 2, and their physical layout in operation is shown in Figure 3.

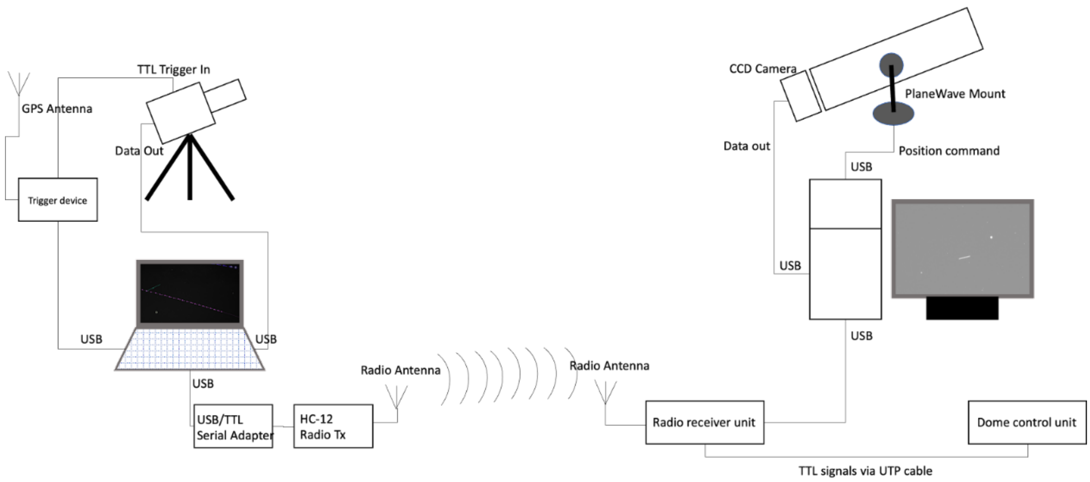

Figure 2. The observation setup – structure of the two observing systems.

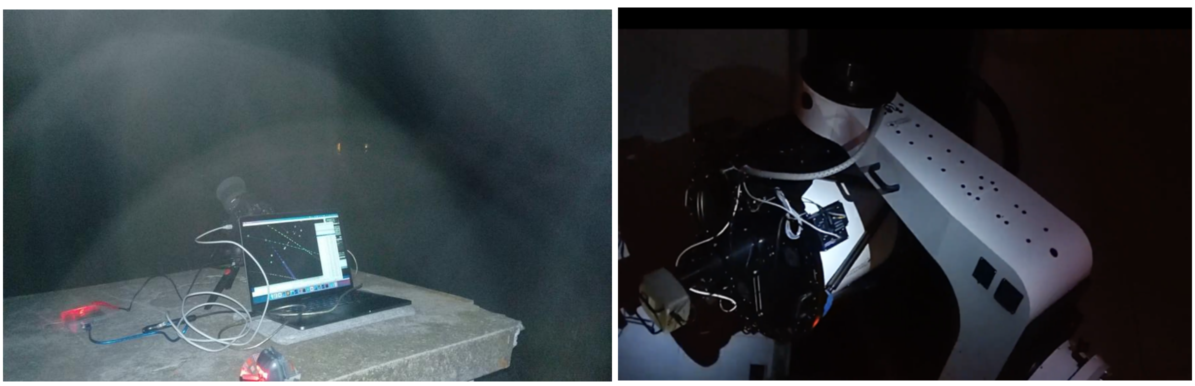

Figure 3. The observation setup: the two systems in operation.

The *radio receiver unit* is essential for the automatization of the whole stare and chase process. This custom-built device has two roles: it is an interface to receive the predictions from the wide FOV observation system, and also the interface to the dome orientation system. The schematic of this device is shown in Figure 4. The central part of the system is the Arduino Mega microcontroller board, which has four hardware serial (UART) communication interfaces, two of them being used by the device. One interface goes through a USB/UART adapter and is used for communicating with the computer, and the other is connected to the HC-12 radio transceiver. The microcontroller board is also connected to a RJ45 connector, into which a UTP cable is plugged. This cable connects the radio receiver unit to the dome control unit, using three wires: a common ground wire, a left turn command wire, and a right turn control wire.

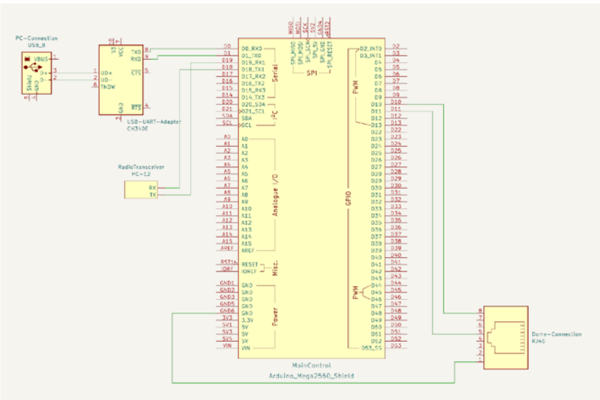

Figure 4. Electric schematic – radio receiver unit.

The *dome control unit* is the hardware interface between the computer-based image acquisition system and the dome of the Astronomical Observatory located in the Feleacu observation site. The dome is rotated by a triphasic electrical motor, which has a two-button control panel that commands the rotations clockwise (right) or counterclockwise (left). In order to automate the rotation of the dome, we have overridden the dome control panel using two relays connected to a microcontroller board. The dome control unit's electrical schematic is shown in Figure 5. The device works in two modes, manual and automatic, and the modes are selected by the Button_Manual switch. In the manual mode, the device works as the existing two-button control panel of the dome. In the automatic mode, the dome rotates based on the commands received via the UTP cable, from the radio receiver unit, which in turn is commanded by the image acquisition PC.

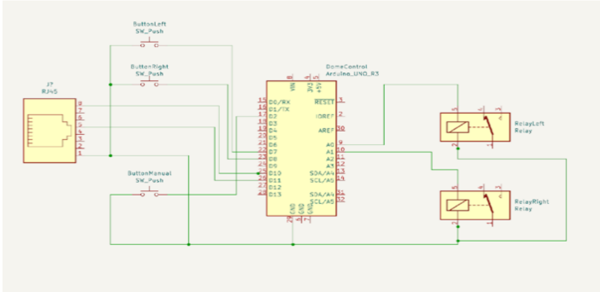

Figure 5. Electric schematic – dome control unit.

4 SYSTEM OPERATION

4.1 Operation of the wide FOV system

The wide FOV system's camera is triggered at a 6 seconds interval, with an exposure time of 3 seconds. This will ensure that the satellite streaks are long enough to be detected and the background stars are bright enough to be identified. The software will then analyse the differences between consecutive frames, looking for motion. Elongated motion areas are selected as satellite streak candidates. Some false positives, due to the apparent motion of the background stars in the absence of sidereal tracking, or due to clouds, can be present at this stage. Next, the satellite candidates are joined into tracklets, using collinearity criteria. Only when at least three streak candidates are joined into a tracklets the software will consider the detections to be valid satellites. More details about the detection process can be read in [9].

For a valid tracklet, predictions for the streak position in future frames is computed, using a simple linear motion model (the average speed, in pixels per frame, is computed, and this speed is used to extrapolate the positions for the next 10 frames). If more targets are observed at the same time, the longest tracklet is selected for result communication to the narrow FOV system.

The process is described in Figure 6. On the left, a crop of the original image is shown, and on the right, we can see that three tracklets are currently active. The empty circles denote predictions for all active tracklets, and the filled, white circles denote the 1-minute lookahead predictions for the selected tracklet. The fifth position, corresponding to a 30 seconds future interval, will be send to the narrow FOV system.

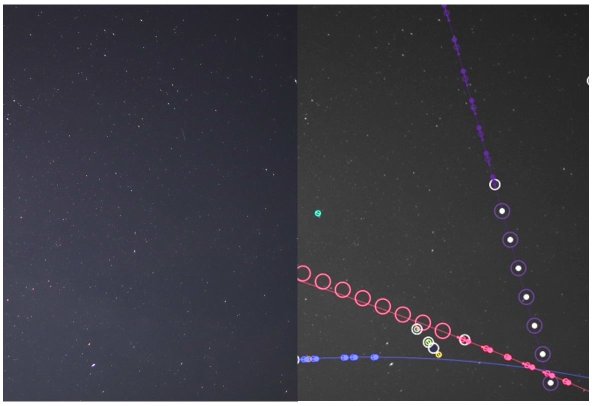

Figure 6. Left – region of the original captured image; Right – tracklets and predictions. The filled white circles denote the selected predictions that will be sent to the telescope.

The telescope requires Right Ascension (RA) and Declination (DEC) celestial coordinates for orientation, and therefore the wide FOV system has to obtain these coordinates for the predicted pixel coordinates of the tracklets. Therefore, astrometric reduction becomes necessary. Due to the fact that we need to have a system that can be set up anywhere, and oriented towards any point of the sky, we have chosen to use the astrometry.net software package [10] to perform blind astrometric calibration for the acquired images. However, the reduction process can be time consuming, and will not usually fit in the 6 seconds interval between acquired frames. On the other hand, the lack of sidereal tracking means that the starry background will not be the same throughout the whole observation time. Thus, a compromise had to be made:

- The detection process and the astrometry calibration process (generation of world coordinate files, .wcf) will run in parallel.
- The astrometry calibration process is invoked at a 4 minutes (40 frames) interval. This leaves the calibration process enough time to complete.
- When computing the RA/DEC coordinates for the predictions, the most recent calibration file (.wcf file) is used. The file is timestamped with the time of the image used for calibration. The difference in time between the calibration time and the prediction time is used to correct the RA coordinate, at a rate of 15 arcseconds for 1 time second.

Due to this compromise, we obtain the celestial coordinates quickly, but the accuracy is less than ideal. Fortunately, it is enough to orient the telescope so that the satellite will pass through its FOV.

The wide FOV system will send a single predicted position (RA, DEC) to the telescope system, using the radio interface. We have selected to send the position predicted 30 seconds into the future. This time interval is another compromise: it has to be long enough to account for the latency of the processing (time of acquisition and processing), for the time needed for the telescope to be oriented, and for the dome to rotate to align with the telescope. On the other hand, a time that is too long will lead to prediction errors, especially if the trajectory of the satellite is not linear.

In order to avoid overloading the telescope orientation system, we will only send at most one prediction per minute. Therefore, after a successful sent prediction, we have a 60 seconds, or 10 frames, cooldown.

4.2 Operation of the narrow FOV system

The narrow FOV observation system is normally used for tracking, using known orbital information for predicting passes of different satellites of interest. This activity, part of the EUSST effort, must not be affected by the added surveillance capabilities. We have designed a software component that handles the telescope positioning taking by into account both situations: the planned observations and the random targets discovered by the wide FOV system. The planned observations are a sequence of RA/DEC coordinates with associated timestamps. The system will process them in order, orienting the telescope at the proper times, and no other interference is allowed 30 seconds before and after the specified timestamp. This way, we ensure that the planned observation sequence is not disturbed.

The telescope orienting software receives data, in the form of RA/DEC coordinates, plain text, from the radio receiver unit. If the reception happens when the system is within +-30 seconds of a planned observation, the received data is ignored. Otherwise, the telescope is oriented towards the received coordinates.

The image acquisition process is controlled by a MaxImDL software. The images, 16-bit monochrome FITS files of 768x512 pixels in size (binning mode), are acquired every two seconds, with an exposure time of 1 second. The images are precisely timestamped, and the file metadata contains the RA/DEC coordinates where the telescope has been oriented. The PlaneWave L600 mount operates in sidereal tracking, ensuring a fixed star background.

The image acquisition process is continuous, and will not be interrupted by successive orientations of the telescope, caused by programmed observations or by the data received from the wide FOV system. The splitting of the sequence into subsequences of constant star background is achieved after the experiment is completed, based on the metadata. A change in the RA or DEC of the field centre signals a new subsequence. Each subsequence will be processed independently, as it requires independent astrometric calibration.

The algorithm for detecting satellite streaks in the subsequences is the same algorithm used for the wide FOV system, with adjusted settings for streak candidate validation, taking into account the different apparent size of the streak in the two types of images. The sidereal tracking mode, and the offline processing which allows us to use multiple calibration files for a subsequence, ensure that the accuracy of the narrow field sequences approaches the limits defined by the pixel angular error.

An example of a tracklet result from a narrow field image sequence is shown in Figure 7. The narrow FOV of the system, 1.98x1.32 degrees, limits a typical LEO pass to 2 … 10 observable frames, depending on the distance.

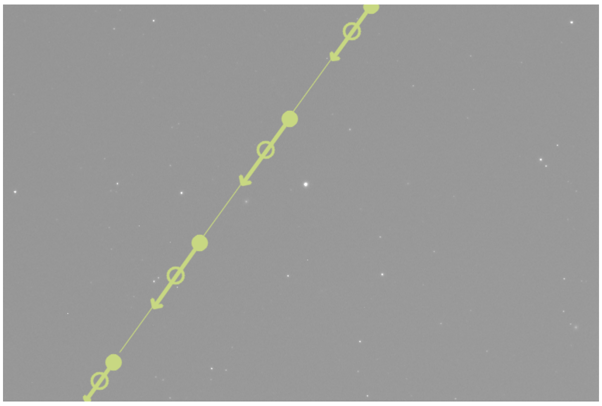

Figure 7. A tracklet detected from a narrow FOV image sequence.

4.3 Automatic dome orientation

The hardware components for dome orientation are described in chapter 2. The dome control unit is able to command the motor that moves the heavy, 6m diameter main dome of the Observatory, to bring it in alignment with the telescope. The dome control unit is connected by cable to the radio receiver unit, which is also connected to the image acquisition PC, which runs the image capturing software MaxImDL [11] and the custom telescope orienting software. We have included the dome control logic in the same software module that controls the telescope and receives the prediction coordinates. One of the reasons is that the program is already connected via the serial over USB interface with the radio receiver unit, for receiving the commands, and it was easy to make it also give commands to the unit, for rotating the dome. Therefore, by simple, plain text commands (*L* – rotate left, *R* – rotate right, *C* – center, stop) issued via a serial USB port, the telescope control program can also command the dome.

Now that we have provided a means to provide commands to the dome, we need the following two important pieces of information for control:

- What is the direction of the last movement of the telescope?
- Is the telescope aligned with the dome?

The dome does not have any sensors to provide the current alignment. However, the ASCOM compatible driver of the telescope's PlaneWave L 600 mount is able to provide us, in real time, the azimuth angle, after the telescope moves to the specified RA/DEC coordinates. Therefore, we can infer at least the sense of rotation and the angular difference from the last stable position of the telescope, and therefore we can decide the best sense of rotation of the dome.

The decision whether to start moving the dome, and when to stop moving it, is now based on whether the telescope is aligned to the dome's opening or not. For this, we will use the average brightness of the acquired FITS images. When the telescope is pointing towards the dome, the interior ambient red light causes a much brighter image than the night sky. An average intensity is computed at the start of the experiment, with the dome manually aligned to the telescope. When the telescope is moved and it becomes pointed towards the dome's interior, a significant increase of image intensity is detected. The dome is rotated based on the azimuth different angle, and the rotation stops when the average intensity becomes low again. A sequence of images caused by misalignment of the telescope to the dome is shown in Figure 8. The first image is stable, the second image is captured while the telescope is moving to a new position, and the third image is captured when the telescope points towards the walls of the dome. At this point, the dome will be commanded to rotate.

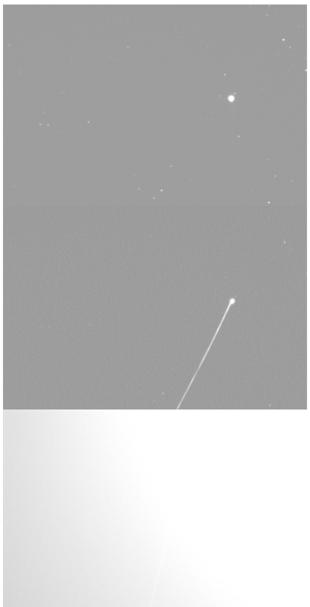

Figure 8. Detecting the misalignment: top – stable image, middle – telescope is moving, bottom – telescope points towards the walls of the dome.

This approach has the advantage of not requiring additional hardware mounted on the telescope or on the dome. The main disadvantage is that the feedback mechanism is relatively slow, being dependent on the rate of image acquisition (one frame every two seconds).

5 ALTERNATIVE SETUP FOR THE WIDE FOV SYSTEM

Recently, we have experimented with a new configuration for the wide FOV system, using a new lens for the DSLR camera. The new lens is a Canon EF 85mm f/1.8 USM, having a 85 mm focal length and the same aperture as the previous lens. The image size remains at 2400x1600 pixels, and the new angular accuracy, determined by astrometric calibration is at 23 arcseconds/pixel, four times more precise than the initial configuration. The camera can be configured to acquire images up to a size of 6000x4000 pixels, which would lead to an accuracy of 9.13 arcseconds/pixel, but these images are too large to be processed in real time to be useful for predicting the satellite trajectories for orienting the telescope system. Also, the lack of sidereal tracking means that this theoretical precision will not be achieved anyway.

The new setup has an angular FOV of 15x10 degrees, considerably smaller than the initial setup, but still much larger than the telescope's.

The new angular resolution implies longer streaks for the satellites, and also a more pronounced elongation of the stars, due to the absence of sidereal tracking. For these reasons we have reduced the exposure time to 1.5 seconds, and the time interval between the frames to 3 seconds instead of 6. We have also increased the camera gain factor (ISO), experimenting with the values 1600 and 3200, so that we can detect satellites which are further away, to the upper limit of the LEO region.

6 RESULTS

We have performed multiple tests with both the 20 mm and the 85 mm lenses, but many tests were of short extent, as the window of opportunity for the LEO observation is quite small after the sunset, and the weather conditions were often changing, and sometimes the clear sky was limited to a small region, or quickly became cloudy. We have selected the most representative tests for both lens configurations to describe in the next sections.

6.1 Results with the 20 mm lens

On 21.06.2022 we have performed a two hour experiment, starting from 20:05 UTC and ending at 22:07 UTC (local time interval 23:03 – 01:07). During this time, the wide FOV system, equipped with the 20 mm lens, detected 144 tracks, out of which 123 were later validated to belong to known satellites, based on the most recent complete TLE file downloaded from space-track.org. The remaining 21 tracks were not identified, some of them belonging to planes, as the Cluj-Napoca area has a busy air traffic, or they may belong to space debris with highly outdated orbital information.

Based on the predictions generated by the wide FOV system, the narrow FOV system was able to detect 64 tracks. Most of the satellites were detected by the telescope in a single pass (therefore generating a single track file), but several, more distant and therefore having a lower angular speed, were detected in two or even three passes.

We were not able to use all the wide FOV detections as successful predictions for the telescope system, due to the following factors:

- The simultaneous presence of multiple satellites in the wide FOV will cause only one to be used for prediction, and the others will not be observed by the telescope.
- The validation conditions for the prediction are that the satellite was previously detected in at least 4 frames, and that it is detected in the current frame. Some satellites, of variable intensity, may be missed this way.
- The 1 minute cooldown between predictions.
- Some high speed satellites may traverse the narrow FOV too quickly, and sometimes their pass will not cause at least two full length streaks for the tracklet to be validated.
- The trajectories of the satellites in the wide FOV are often not linear motions, and therefore the predicted positions at 30 seconds in the future can be erroneous and the telescope can miss the pass. This is the main problem with the 20 mm lens, as the FOV is very wide and the nonlinearity of the trajectories is sometimes quite pronounced.

In figures 9, 10, 11, 12 we can see the passes of the CZ-4C DEB space debris, NORAD ID 40343, a LEO object of eccentric orbit, the distance between the ground surface varying between 900 and 1300 km. In figures 9 and 11 we can see the wide FOV detections and the predictions for the first and for the third pass, and in figures 10 and 12 we can see the telescope images of the satellite's passes.

The narrow FOV images were processed offline, after the completion of the experiment, and the results were compared to the predicted positions from the orbital elements. The results of narrow FOV processing, along with the results of the wide FOV processing and the predictions from the orbital elements are shown in Figure 13. We can see that as the object approaches the bottom right of the wide FOV image, the accuracy of the results decreases, but the narrow FOV results remain accurate.

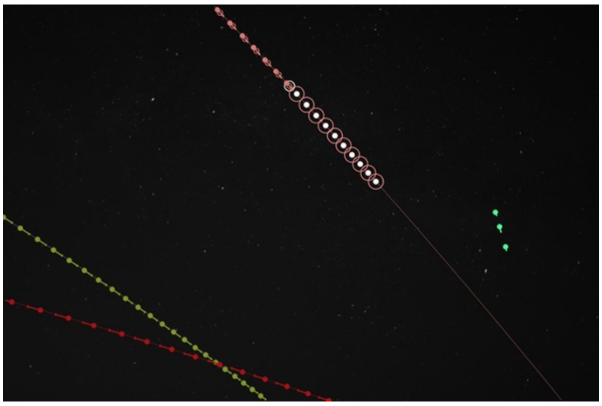

Figure 9. Detection using the wide FOV with the 20 mm lens, and prediction for the first telescope pass.

Figure 10. The first telescope pass of the CZ-4C DEB object through the telescope's FOV.

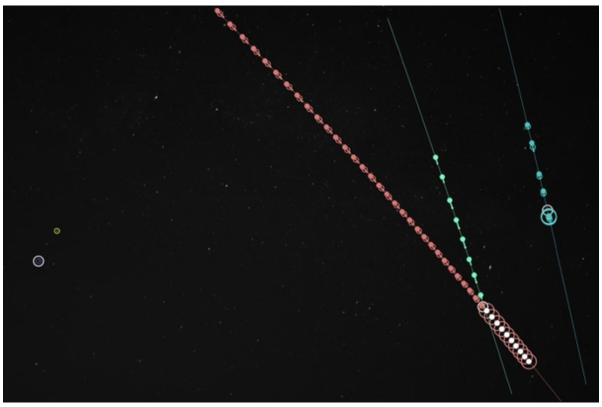

Figure 11. Detection using the wide FOV with the 20 mm lens, and prediction for the third telescope pass.

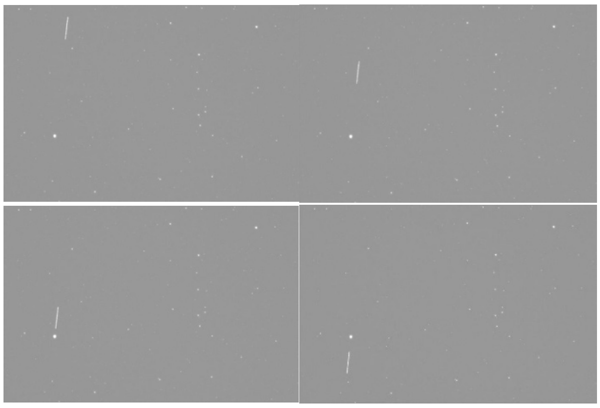

Figure 12. The third telescope pass of the CZ-4C DEB object through the telescope's FOV.

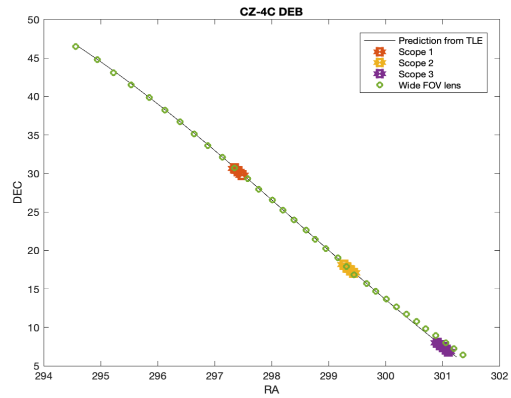

Figure 13. Comparison of the trajectories – the long trajectory of the wide FOV detection, and the three short trajectories for the three passes through the telescope's FOV. The continuous line is the prediction from the orbital elements.

6.2 Results with the 85 mm lens

During an experiment conducted in 29.11.2022, between local time 18:20 and 19:20 (UTC time 16:20 – 17:20), limited to a single hour due to heavy clouding later on, the wide FOV system detected, in live processing mode, 50 satellites, and the narrow FOV system, oriented by the predictions, was able to detect correctly 20 satellites. The difference between the two numbers is caused by the following factors:

- The simultaneous presence of multiple satellites in the wide FOV will cause only one to be used for prediction, and the others will not be observed by the telescope.
- The validation conditions for the prediction are that the satellite was previously detected in at least 4 frames, and that it is detected in the current frame. Some satellites, of variable intensity, may be missed this way.
- The 1 minute cooldown between predictions.
- Some high speed satellites may traverse the narrow FOV too quickly, and sometimes their

pass will not cause at least two full length streaks for the tracklet to be validated.

- The 5 frame lookahead, which was used for the 20 mm lens with 6 seconds frame interval, was not updated, and therefore the 30 seconds of prediction became 15 seconds. Sometimes, this caused the satellite to pass when the telescope was still in motion, and therefore to not be detected.

We will analyse and tune the parameters of the system to better use the new lens setup.

A sample result of the new setup is shown in Figures 14, 15 and 16. The GLOBALSTAR M086 satellite orbits in the upper part of the LEO region, at 1500 km above the surface of the Earth, and therefore has a lower angular speed, and could be observed for three passes using the telescope and the predictions. We have used a camera ISO of 3200 for the large FOV system, which increased sensitivity and therefore allowed us to detect distant LEOs, but also increased the noise level in the image, as Figure 14 shows. This figure also shows that at least two satellites are active at the same moment, and 6 trajectories are recent enough that their prediction may be suppressed by the cooldown period. In Figure 15 we can see the four frames of the last pass in the FOV of the telescope.

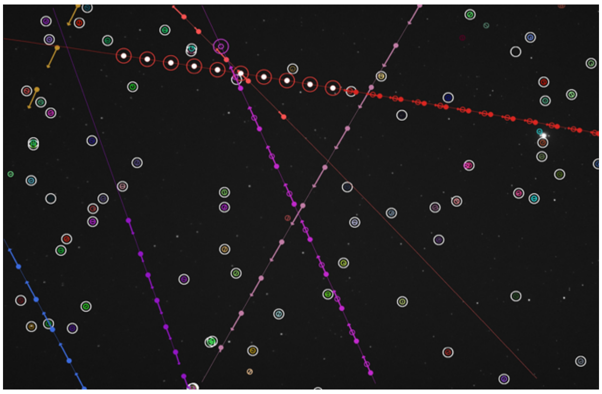

Figure 14. Detection using the wide FOV with the 85mm lens.

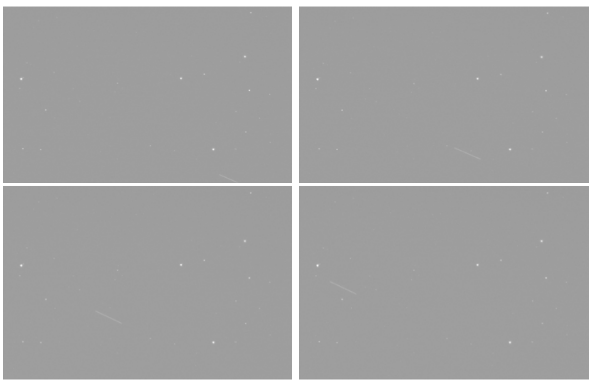

Figure 15. The third pass of the GLOBALSTAR M086 satellite through the telescope's FOV.

Using the satellite's known orbital parameters, downloaded from space-track.org, we have joined the four observations (the wide FOV track and the three narrow FOV tracks) and compared them to the predicted trajectory. The results are shown in Figure 16.

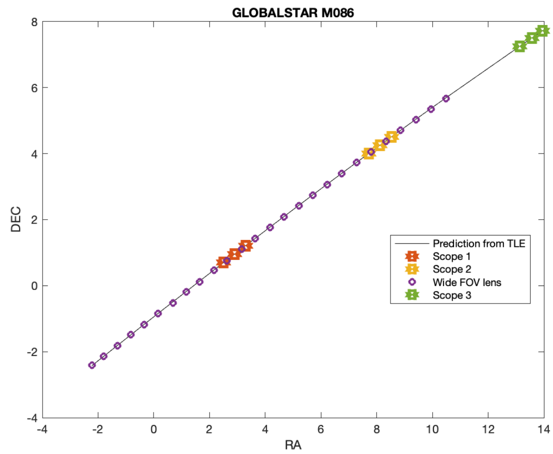

Figure 16. Comparison of the trajectories – the long trajectory of the wide FOV detection, and the three short trajectories for the three passes through the telescope's FOV. The continuous line is the prediction from the orbital elements.

7 DISCUSSION

The main advantage of the 20 mm lens setup is the extremely wide FOV, 60x40 degrees, a very wide area of the sky. This wide FOV can be useful for detecting orbiting objects that have extremely outdated orbital parameters, or which are in a process of atmospheric re-entry, with rapid orbital decay. The wide FOV comes also with several disadvantages:

- The wider angular size of the pixel means a shorter streak, and also a lower brightness for the individual pixels. This means that the 20 mm setup will not work reliably for more distant or fainter objects.
- The wide FOV leads to highly non-linear trajectories, which are sometimes difficult to extrapolate to generate useful predictions. For this reason, some trajectories detected with the 20 mm wide FOV were not confirmed by the telescope.
- The width of the FOV is much higher than the opening of the dome, meaning that the dome had to move often, which lead to more delays, which increase the time of the prediction. This time increase, combined with non-linear trajectories, increase the chance of false predictions and missed trajectories.

The 85 mm lens setup has a smaller FOV, of only 15x10 degrees, and, for the same number of pixels, a smaller angular pixel size. This means higher accuracy and higher sensitivity. The longer streaks allowed us to reduce the exposure time and increase the frame rate, and the resulted trajectories are much closer to a linear trajectory, reducing the prediction errors. The opening of the dome is similar to the width of the 85 mm setup FOV, meaning that most of the time the dome did not require movement. Also, when analysing the throughput of the two systems, we find them to be quite similar, as the loss of FOV is compensated by the increase of sensitivity.

More tests are required, in various conditions and for different types of applications. The 20 mm wide FOV system can be used for guiding the telescope to survey brighter objects on a wider area, and for re-entry events, while the 85 mm system can be used for narrowing down the surveillance to a smaller patch of the sky, but with increased chances of detecting fainter objects.

8 CONCLUSION AND FUTURE WORK

In this paper we have presented a solution for LEO objects surveillance based on wide FOV detection followed by narrow FOV tracking. Our work started from an existing and operational tracking system, which needs to retain all its capabilities and also to remain operational during our experiments. For this reason, we focused on developing the wide FOV system as a portable system, that can be set up anywhere outside of the main dome of the Observatory in about 10 minutes, without need for power sources, data cables or star tracking mounts. Once the portable system is started, it can send prediction data using a radio interface, which has enough range to cover all the Observatory's compound. The predictions will not interfere with programmed tracking sessions, as they will be ignored when the telescope is busy.

We have experimented with two lens setups, each having advantages or disadvantages. Overall, there is no downside of using any of the wide FOV solutions along with the telescope tracking system, as it can only increase the number of measurements that can be performed in a given amount of time.

Future work will be focused on three main directions:

- Improving the quality of object detection, especially by removing the planes. Sometimes, planes cause streaks similar to the satellites, and predictions based on these streaks will waste precious observation time.
- Improving the quality of predictions: we will attempt to better model the non-linear trajectories, so that the larger FOV can be used to their full potential.
- Designing a better target priority mechanism. So far we select the oldest track to be extrapolated for narrow field observations, but in the future we can incorporate additional criteria, such as possible trajectories of objects of interest, or we can exclude objects of specific trajectories.

9 ACKNOWLEDGMENT

The research was supported by a grant from the Ministry of Research and Innovation, CNCS–UEFISCDI, project number PN-III-P2-2.1-SOL-2021-2-0192, within PNCDI III, and a grant from European Commission, Research Executive Agency, Specific Agreement Number 952852 – 2-3SST2018-20.

10 REFERENCES

1. European Space Agency (2021). *Database and information system characterising objects in space*, https://discosweb.esoc.esa.int/. Accessed: 2023-01-17.

2. ESA Space Debris Office (2022). *ESA's Annual Space Environment Report*, GEN-DB-LOG-00288-OPS-SD, Issue 6.0, ESA/ESOC, Darmstadt, Germany.

3. Haimerl, J.A. & Fonder, G.P. (2015). Space Fence System Overview. *Proceedings of the 16th AMOS (Advanced Maui Optical and Space Surveillance Technology Conference)*, USA, Sept. 5-18, 2015. http://www.amostech.com/TechnicalPapers/2015/SSA/Haimerl.pdf. Accessed: 2023-01-17.

4. Boër, M., Klotz, A., Laugier, R., Richard, P., Dolado Perez, J.-C., Lapasset, L., Verzeni, A., Théron, S., Coward, D.& Kennewell, J.A. (2017). TAROT: A network for Space Surveillance and Tracking operations. *Proceedings of 7th European Conference on Space Debris*, Darmstadt, Germany. https://conference.sdo.esoc.esa.int/proceedings/sdc7/paper/382/SDC7-paper382.pdf. Accessed: 2023-01-17.

5. Bland, P., Madsen, G., Bold, M., Howie, R., Hartig, B., Jansen-Sturgeon, T., Mason, J., McCormack, D.& Drury, R. (2018). FireOPAL: Toward a Low-Cost, Global, Coordinated Network of Optical Sensors for SSA. *Proceedings of the 19th AMOS (Advanced Maui Optical and Space Surveillance Technology Conference)*, USA, Sept. 5-18, 2015. https://amostech.com/TechnicalPapers/2018/Optical-Systems_Instrumentation/Bland.pdf. Accessed: 2023-01-17.

6. Danescu, R., Oniga, F., Turcu, V.& Cristea, O. (2012). Long Baseline Stereovision for Automatic Detection and Ranging of Moving Objects in the Night Sky. *Sensors* **12**(10), 12940-12963.

7. Hasenohr, T. (2016). *Initial Detection and Tracking*

of Objects in Low Earth Orbit. Master Thesis, German Aerospace Center Stuttgart, University of Stuttgart, Institute of Applied Optics. Available online: https://elib.dlr.de/110661/1/Initial%20Detection%20and%20Tracking%20of%20Objects%20in%20Low%20Earth%20Orbit.pdf. Accessed:2023-01-17.

8. Balan, M., Apostol, A.R., Cherciu, C., Turcu, V., Nedelcu, D.A., Trelia, M.M. & Mihai, S.-Ș. (2022). Synoptes – Precise GNSS Timestamping Device for Space Surveillance and Tracking Observations. *20th IAA Symposium on Space Debris (A6), 73rd International Astronautical Congress*, 2022, Paris, France. Paper ID: 68551. https://iafastro.directory/iac/paper/id/68551/abstract-pdf/IAC-22,A6,IP,20,x68551.brief.pdf?2022-04-05.10:50:40, Accessed:2023-01-17.

9. Danescu, R.G., Itu, R., Muresan, M.P., Rednic, A.& Turcu, V. (2022). SST Anywhere – A Portable Solution for Wide Field Low Earth Orbit Surveillance. *Remote Sensing,* **14** (8), art no. 1905.

10. Roweis, S., Lang, D., Mierle, D., Hogg, D.& Blanton, M. Making the Sky Searchable: Fast Geometric Hashing for Automated Astrometry. https://cosmo.nyu.edu/hogg/research/2006/09/28/astrometry_google.pdf; http://astrometry.net. Accessed:2023-01-17.

11. Keller, W.A. (2014). *Getting Started with MaxImDL 6*, Diffraction Limited, https://cdn.diffractionlimited.com/downloads/GettingStarted.pdf. Accessed:2023-01-17.